Biomaterials Science

ROYAL SOCIETY OF CHEMISTRY

PAPER

View Article Online
View Journal | View Issue

Published on 26 December 2019. Downloaded by Universita Degli Studi di Napoli Federico II on 1/11/2024 3:00:47 PM.

Check for updates

Cite this: *Biomater. Sci.*, 2020, **8**, 1329

Enhancing doxorubicin anticancer activity with a novel polymeric platform photoreleasing nitric oxide†

Federica Sodano, *[a] Robert J. Cavanagh,‡[b] Amanda K. Pearce, ‡[b] Loretta Lazzarato, [a] Barbara Rolando, [a] Aurore Fraix, [c] Thais F. Abelha, [b] Catherine E. Vasey,[b] Cameron Alexander, [b] Vincenzo Taresco *[b] and Salvatore Sortino *[c]

Combinations of conventional chemotherapeutics with unconventional anticancer agents such as reactive oxygen and nitrogen species may offer treatment benefits for cancer therapies. Here we report a novel polymeric platform combining the delivery of Doxorubicin (DOXO) with the light-regulated release of nitric oxide (NO). An amphiphilic block-copolymer (P1) was designed and synthesized as the drug carrier, with pendant amine groups to attach DOXO *via* a urea linkage and a NO photodonor (NOPD) activable by visible light. The two grafted-copolymers (P1-DOXO and P1-NOPD) self-assembled *via* solvent displacement methods into nanoparticles (NPs), containing both therapeutic components (NP1) and, for comparison, the individual NOPD (NP2) and DOXO (NP3). All the NPs were fully characterized in terms of physicochemical, photochemical and photophysical properties. These experiments demonstrated that integration of the NOPD within the polymeric scaffold enhanced the NO photoreleasing efficiency when compared with the free NOPD, and that the proximity to DOXO on the polymer chains did not significantly affect the enhanced photochemical performance. Internalization of the NPs into lung, intestine, and skin cancer cell lines was investigated after co-formulation with Cy5 fluorescent tagged polymers, and cytotoxicity of the NPs against the same panel of cell lines was assessed under dark and light conditions. The overall results demonstrate effective cell internalization of the NPs and a notable enhancement in killing activity of the dual-action therapeutic NP1 when compared with NP2, NP3 and the free DOXO, respectively. This suggests that the combination of DOXO with photoregulated NO release, achieved through the mixed formulation strategy of tailored polymer conjugate NPs, may open new treatment modalities based on the use of NO to improve cancer therapies.

Received 15th October 2019,
Accepted 23rd December 2019

DOI: 10.1039/c9bm01644a

rsc.li/biomaterials-science

Introduction

Multimodal cancer therapy involves the use of two or more treatment modalities with the aim to attack tumors by acting either on a single oncogenic pathway through different mechanisms or across parallel pathways without amplification of side effects.[1–7] In this regard, the combination of conventional chemotherapeutics with light-activated release of oxidizing agents such as reactive oxygen and nitrogen species (ROS and RNS) may open new routes to better therapies.[8] Light is a minimally invasive tool that permits the introduction of a cytotoxic burst in biological environments with high spatiotemporal control.[9] Among the light activatable therapeutic treatments, photodynamic therapy (PDT) is so far one of the most promising to combat cancers.[10] PDT is based on the catalytic photogeneration of the highly reactive singlet oxygen ($^1O_2$) through appropriate photosensitizers (PSs) and combinations of PDT with chemotherapy have been successfully demonstrated for multimodal cancer treatments.[11] Another emerging light-activated approach is based on the photoregulated release of nitric oxide (NO) through the use of NO photodonors (NOPDs).[12–16] Although still confined to the research area, NO-based PDT, namely NOPDT, has very promising features for cancer treatment.[17] In fact, NO, apart from playing multiple roles in the

[a]*Department of Drug Science and Technology, University of Turin, 10125, Turin, Italy. E-mail: federica.sodano@unito.it*
[b]*School of Pharmacy, University of Nottingham, NG7 2RD, UK. E-mail: Vincenzo.Taresco@nottingham.ac.uk*
[c]*Laboratory of Photochemistry, Department of Drug Sciences, University of Catania, I-95125 Catania, Italy. E-mail: ssortino@unict.it*

†Electronic supplementary information (ESI) available. See DOI: 10.1039/c9bm01644a

‡These authors contributed equally.

Published on 26 December 2019. Downloaded by Universita Degli Studi di Napoli Federico II on 1/11/2024 3:00:47 PM.

bioregulation of a broad array of physiological processes,[18] has also proven to play a key role in cancer biology.[19] This diatomic radical is a multitarget species able to attack proteins, lipids and DNA, does not incur multi-drug resistance (MDR) and, in view of its short lifetime (*ca.* 5 s in tissues) is confined to a tightly-defined region of action, reducing systemic off-target effects typical of many conventional drugs. However, the biological effects of NO in cancer are strictly dependent on its concentration.[19] For example, low levels of NO (in the pM–nM concentration range) inhibit apoptosis.[20] On the other hand, high levels of NO (μM concentration range) promote apoptosis directly through nitrosylation of crucial mitochondrial enzymes,[21,22] or indirectly, *via* oxidative and nitrosative stress resulting from the formation of RNS.[23] Furthermore, in a concentration range not sufficient either to inhibit or encourage apoptosis, NO has been revealed to be very effective in inhibiting the ATP Binding Cassette (ABC) transporters, which in turn regulate the efflux of chemotherapeutics and induce MDR in cancer cells.[24,25] For such reasons, the NOPDs are more appealing as therapeutic agents rather than NO precursors releasing NO upon thermal, enzymatic or metabolic stimuli.[26,27] In fact, NOPDs allow NO dosage to be controlled with great accuracy by tuning the duration and intensity of the irradiation. In contrast to PDT, the working principle of NOPDT is not catalytic as it exploits the excitation light to uncage NO leading to a consumption of the NOPD.[12–16] However, since NO photorelease is independent of O_2 availability, NOPDT offers the great advantage to successfully complement PDT at the onset of hypoxic conditions, typical for some tumours, where PDT may otherwise fail.[28] This has made combinations of NOPDT with conventional PDT a subject of much investigation in recent years.[29] However, there are surprisingly limited examples in which the combination of NOPDT with chemotherapeutics have been reported to date.[30]

Doxorubicin (DOXO) is one of the most widely-adopted anticancer drugs among anthracycline derivatives.[31] However, its effectiveness is limited by a series of resistance mechanisms that usually occur regardless of the nature of the tumor. In a resistance condition, the energy-dependent drug efflux pumps (*i.e.*, P-gp, MDR-related protein 1 and breast cancer resistance protein) actively efflux DOXO from the cells, hence, reducing its pharmacological potential. We have recently demonstrated the successful combination of NOPDs with DOXO as a suitable strategy to fight MDR, increasing the intracellular accumulation of DOXO, enhancing its activity and significantly reducing its active concentration.[30] Despite the current clinical standards of "cocktail administrations" using combinations of drugs, in the case of an antineoplastic agent with NOPD, there are significant pharmacokinetic and pharmacodynamic limitations as a result of the distinctive physiological fates and non-uniform distribution of the free drugs. Accordingly, the development of nanocarrier materials, in which multiple therapeutic cargoes can be entrapped in a single nanoparticle agent, is a promising approach for synchronizing and optimizing the location, timing and duration of combination drug release.[32,33] Polymer conjugates in particular offer many possibilities for precise and controlled delivery of multiple therapeutics in the same area of the body and at predefined extra/intracellular levels.[34,35] In this context, we have recently reported the synthesis of biodegradable block copolymers containing polyethylene glycol, lactide and a functionalized protected cyclic carbonate, which self-assemble into nanoparticles (NPs) and which can be functionalized with "active" molecules, such as DOXO.[36] We hypothesized that the anticancer performance of DOXO might be enhanced by exploiting the photoregulated release of NO, and describe herein a multi-component (NOPD-DOXO) polymeric platform which can be assembled by a simple formulation strategy. In the present work, we describe the synthesis, characterization and biological evaluation of these materials in lung, intestinal and skin cancer cell lines, and show their improved efficacy compared to the individual components.

Results and discussion

Polymeric platform: synthesis and characterization

The block copolymer platform used as a drug carrier has been previously described.[36] Methoxy-polyethylene glycol with molecular weight 5000 Da ($mPEG_{5000}$) was used to initiate Ring-Opening Polymerisation (ROP) of co-monomers lactide (LA) and an in-house prepared cyclic carbonate bearing a *tert*-butoxycarbonyl (BOC)-protected amine, named *tert*-butyl (2-oxo-1,3-dioxan-5-yl) carbamate (referred as tBSC) with 1,8-diazabicyclo [5.4.0]undec-5-ene, (DBU)[37] as a catalyst. The final block ratio achieved was $mPEG_{5000}$: (LA) : (tBSC) 1 : (50) : (50) while the resulting architecture was linear. The subsequent conjugation of $mPEG_{5000}$-$(LA)_{50}$-$(tBSC)_{50}$, named P1, with the drugs of our interest, NOPD and DOXO, was performed through two steps, as shown in Scheme 1A–C. The reaction conditions of both steps were previously optimised:[36] initially, the BOC-deprotection was carried out *via* TFA hydrolysis (Scheme 1A) and subsequently, the conjugation of partly deprotected $mPEG_{5000}$-$(LA)_{50}$-$(tBSC)_{50}$, named P1*, with the "active" molecule (DOXO or NOPD) utilized *N*,*N*′-disuccinimidyl-carbonate (DSC) coupling (Scheme 1). Therefore, two grafted-copolymers P1-NOPD (Scheme 1B) and P1-DOXO (Scheme 1C) were produced by a similar synthetic strategy with the only difference in reaction conditions being the solvents used, *i.e.* acetonitrile for P1-NOPD and a mixture of DMSO/acetonitrile, 50/50, v/v for P1-DOXO. The units estimated by ^{1}H NMR spectra of NOPD linked to the polymer were found to be *ca.* 10, while those of DOXO were *ca.* 4.

The choice of using an NOPD based on a nitroaniline-derivative chromophore reported in Scheme 1 was previously developed in our group,[38,39] and has been successfully integrated in a variety of nanoconstructs[40] and presents the following advantages: (i) excellent dark stability and NO release exclusively controlled by illumination with visible light; (ii) chemical derivatization by simple synthetic procedures; (iii) absorption spectrum which does not significantly overlap the

 This journal is © The Royal Society of Chemistry 2020

Published on 26 December 2019. Downloaded by Universita Degli Studi di Napoli Federico II on 1/11/2024 3:00:47 PM.

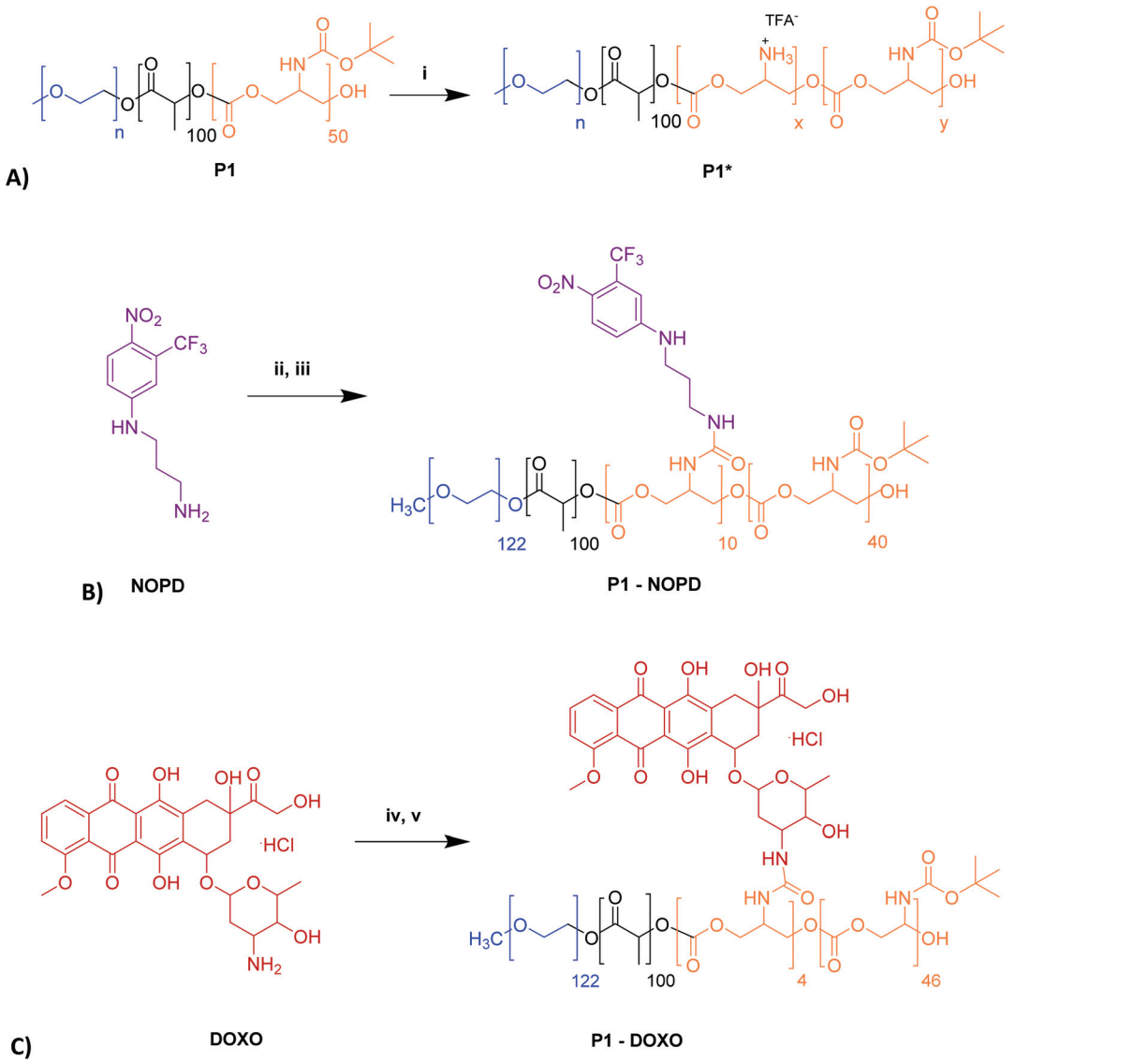

Scheme 1 Reagents and conditions: (A) BOC-deprotection. (i) TFA, DCM, 0 °C. (B) Synthesis of P1-NOPD. (ii) DSC, TEA, CH_3CN, 0 °C; (iii) P1*, TEA, CH_3CN, 0 °C. (C) Synthesis of P1-DOXO. (iv) DSC, TEA, DMSO/CH_3CN, 0 °C; (v) P1*, TEA, DMSO/CH_3CN, 0 °C.

absorption of DOXO, allowing the selective excitation of the NOPD with blue light and its easy quantification as well as that of DOXO by spectrophotometric analysis; (iv) lack of fluorescence emission, which precludes any potential quenching by DOXO *via* Förster Resonance Energy Transfer (FRET) once confined in the close proximity (*i.e.*, within the same NP).

Nanoparticles assembly and characterization

The ability of the two grafted-copolymers (P1-NOPD and P1-DOXO) and the bare polymer P1 to self-assemble into NPs was evaluated,[41] using nanoprecipitation as the standard formulation technique. In particular, a mixed micelles strategy was applied,[42] in which P1 and the polymer prodrugs were co-precipitated alternatively in various combinations as described in Fig. 1. Consequently, the formulation NP1 was a mixed, kinetically trapped, micelle-like nanoparticle and was formed by P1-NOPD and P1-DOXO in equal ratio. The other micelle-like NPs were NP2, consisting of P1-NOPD and bare polymer P1 in equal ratio; NP3, with P1-DOXO and P1 and finally, NP4 which constituted only of the bare polymer backbone without a drug or NO-photodonor. This strategy was thus a simple tool to assemble combination therapy NPs using the same polymeric backbone across all the mixed micelles formulations.[37]

As reported in Table 1, the NPs sizes measured by DLS ranged from 43 to 110 nm, indicating that these were kinetically-trapped species and not 'classical' micelles in that the diameters were much greater than those expected from the likely chain lengths of the individual polymers. The smallest micelles were those of NP4 while the largest was NP1, most likely due to the reduced ability to pack side-chains containing both NOPD and DOXO in the NP1 aggregates compared to the 'bare' polymer chains in NP2. Also the zeta potential of all NPs

Published on 26 December 2019. Downloaded by Universita Degli Studi di Napoli Federico II on 1/11/2024 3:00:47 PM.

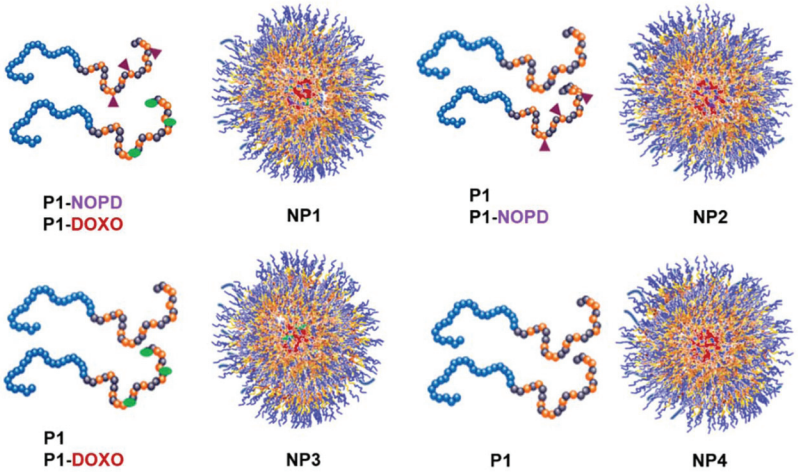

Fig. 1 Schematic illustration of NPs 1–4.

Table 1 Size, zeta potential and polydispersity index (PDI) of NPs 1–4 at 50 μg mL^{-1}

NP	Size ± S.D. (nm)	Zeta potential ± S.D. (mV)	PDI
1	110 ± 10	−25 ± 1	0.242
2	72 ± 7	−20 ± 4	0.111
3	78 ± 3	−19 ± 1	0.132
4	43 ± 5	−14 ± 3	0.092

(Table 1) were negative, ranging from −25 to −14 mV, as expected based on the presence of a hydrophilic PEG corona shell and the weak lone-pair cation interactions at the oxyethylene units and the corresponding association of anions to form the outer layers.[36,41] Interestingly, the smallest micelles had the least negative zeta potential (*ca.* −14 mV) while the NP1 formulations presented the most negative zeta potential value (*ca.* −25 mV), likely indicative of a more expanded PEG corona in the combination micelle-like aggregates. The NPs were stable in biological media (Fig. S1†).

The DOXO or/and NOPD content in each micelle (NP1–3) was evaluated *via* fluorescence or UV detection respectively, and using free DOXO (λ_{exc} = 490 nm, λ_{em} = 553 nm) and NOPD (λ_{max} = 405 nm) as the standard solutions. The amounts of the "active" molecules (DOXO and/or NOPD), expressed as μg mL^{-1}, are reported in Table 2.

Spectroscopic and photochemical characterization of the NPs

Fig. 2A shows the absorption spectrum of NP1 and, for sake of comparison that of the free NOPD and DOXO in water medium. The spectral features reflect the presence of both components in the NPs with the absorption of the NOPD dominating in the blue region and the weaker absorption due to the DOXO in the green region beyond 500 nm. Note that, the absorption maximum of the NOPD in the NPs is blue-shifted of *ca.* 10 nm in comparison to the free NOPD in the same solvent. Since such a shift was also observed in the case of NP2, which did not contain DOXO (see Fig. S2†), it cannot be ascribed to an interaction between the two chromogenic components in the NPs. Rather, in view of the strong push–pull character of the absorption band of the NOPD, which is strongly dependent on the solvent polarity, the shift observed suggests that the NOPD was mainly exposed to a less hydrophilic environment (*i.e.* the inner part of the NPs). Due to the scattering of the NPs, the lower content of DOXO and its low extinction coefficient, compared with the NOPD, it is difficult to gain insights into spectral modification of this component upon binding with the NPs by absorption spectroscopy. Exploiting the fluorescence of DOXO, we then inspected the static and dynamic behaviour of NP1 compared with an optically matched solution of free DOXO. As reported in Fig. 2B, the fluorescence emission efficiency and maxima position of NP1 was very similar to that of the free fluorophore in the same solvent. In addition, the biexponential decay of the free DOXO was only slightly affected upon its binding with the NPs. These results provided evidence that the DOXO-rich regions experienced mainly a hydrophilic environment, as supported by the more negative values of the zeta potential found for NP1 (*vide supra*), and again suggested that these were not sharp core–shell micelles, but trapped aggregates as depicted in the schematics of Fig. 1.

Table 2 NOPD or/and DOXO content in NPs 1–3

NP	DOXO ± S.D. (μg mL^{-1})	NOPD ± S.D. (μg mL^{-1})
1	23.1 ± 2	14.8 ± 1
2	—	28.4 ± 2
3	14.6 ± 1	—

A key requisite for any photoactivatable compound after its integration into appropriate materials, or if used in conjunction with other chromophoric components located in close proximity (*i.e.* NOPD and DOXO), is the preservation of its photochemical properties. This is an important distinction compared to non-photoresponsive compounds and is not

 This journal is © The Royal Society of Chemistry 2020

Published on 26 December 2019. Downloaded by Universita Degli Studi di Napoli Federico II on 1/11/2024 3:00:47 PM.

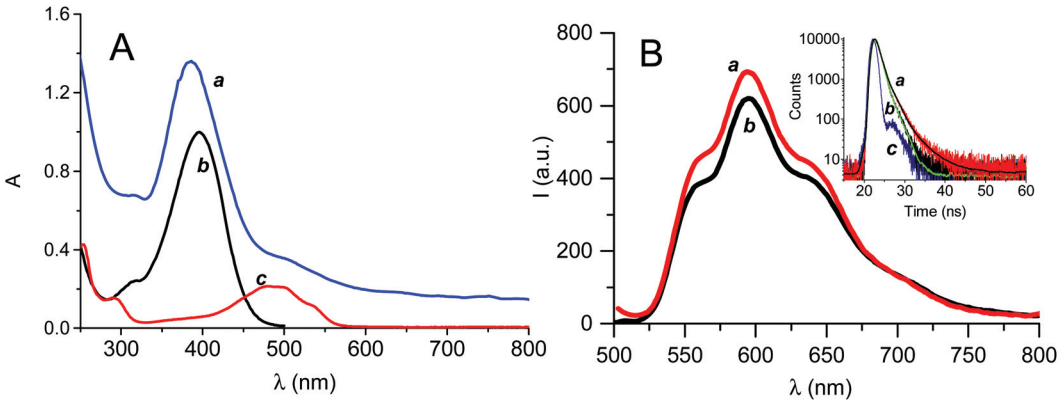

Fig. 2 (A) Absorption spectrum of NP1 (a) and of the equal amounts of free NOPD (b) and DOXO (c) in water. (B) Fluorescence emission spectra (λ_{exc} = 490 nm) of NP1 (a) and of an optically matched solution of free DOXO (b) in water. The inset shows the fluorescence decay and the related bi-exponential fitting for solutions of NP1 (a) and the free DOXO (b); trace c is the prompt signal. λ_{exc} = 455 nm; λ_{em} = 590 nm.

trivial. In most cases, the response to light of the single photoactive units can be significantly affected in nature, efficiency or both by the occurrence of competitive, undesired photoprocesses (*i.e.*, photoinduced energy and/or electron transfer, non-radiative deactivation, *etc.*), which do not allow the photoactivatable components to work independently upon light absorption and therefore preclude the final goal.[32,33] In our case, the non-emissive behaviour of the NOPD helps to avoid any potential quenching by DOXO *via* FRET mechanism. Besides, the localization of the NOPD and DOXO in different environments of the NPs was expected to significantly reduce any dynamic quenching process (*i.e.* energy transfer *via* Dexter mechanism or photoinduced electron transfer).

NO photorelease from NP1, and for comparison NP2, was monitored directly and indirectly through an amperometric technique using an ultrasensitive NO electrode and the Griess assay, which detects the content of nitrite in solution (the main oxidation product of NO), respectively. Fig. 3A shows that NO generation in the micromolar range was exclusively achieved upon visible light excitation, stopped as the light was turned off and restarted when the light was turned on again. Interestingly the NO photogeneration in the NP samples was more than one order of magnitude larger than that observed in aqueous solution for the free NOPD.[38] This result is in excellent agreement to what we recently observed for NOPDs based on the same chromogenic unit entrapped in micellar,[43] calixarene[44] and polymeric nanoassemblies.[45] It is likely that this was due to the low polarity environment experienced by the NOPD (*vide supra*) combined with the presence of easily abstractable hydrogens close to the phenoxy-radical intermediate involved in the mechanism of the NO photorelease.[43–45] It is also worth noting that photoexcitation of the NOPD does not lead to any additional photochemical pathways competitive with the NO photorelease. In fact, as illustrated in Fig. 3B, the spectral changes observed upon irradiations showed a very clear bleaching of the main absorption band of the NOPD, in excellent agreement with the formation of a phenol derivative, absorbing in the UV region, as the sole stable product formed after the NO photogeneration.[38] The slight difference observed in the NO photorelease for the two samples was also confirmed by a Griess assay (Fig. S3†). This was due to a different fraction of absorbed photons by the two samples rather than

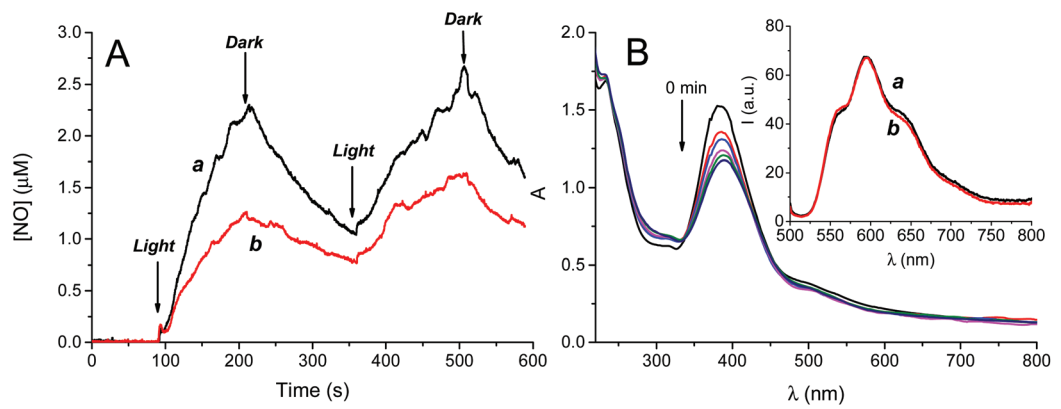

Fig. 3 (A) NO release profile observed for water suspensions of NP2 (a) and NP1 (b); T = 25 °C; λ_{exc} = 405 nm. (B) Absorption spectral changes observed upon 405 nm light irradiation of a water suspension of NP2 for irradiation intervals of 0, 4.5, 6, 7.5, 9 and 10.5 min. The inset shows the fluorescence spectra of the NP2 before (a) and at the end of the irradiation (b).

Published on 26 December 2019. Downloaded by Universita Degli Studi di Napoli Federico II on 1/11/2024 3:00:47 PM.

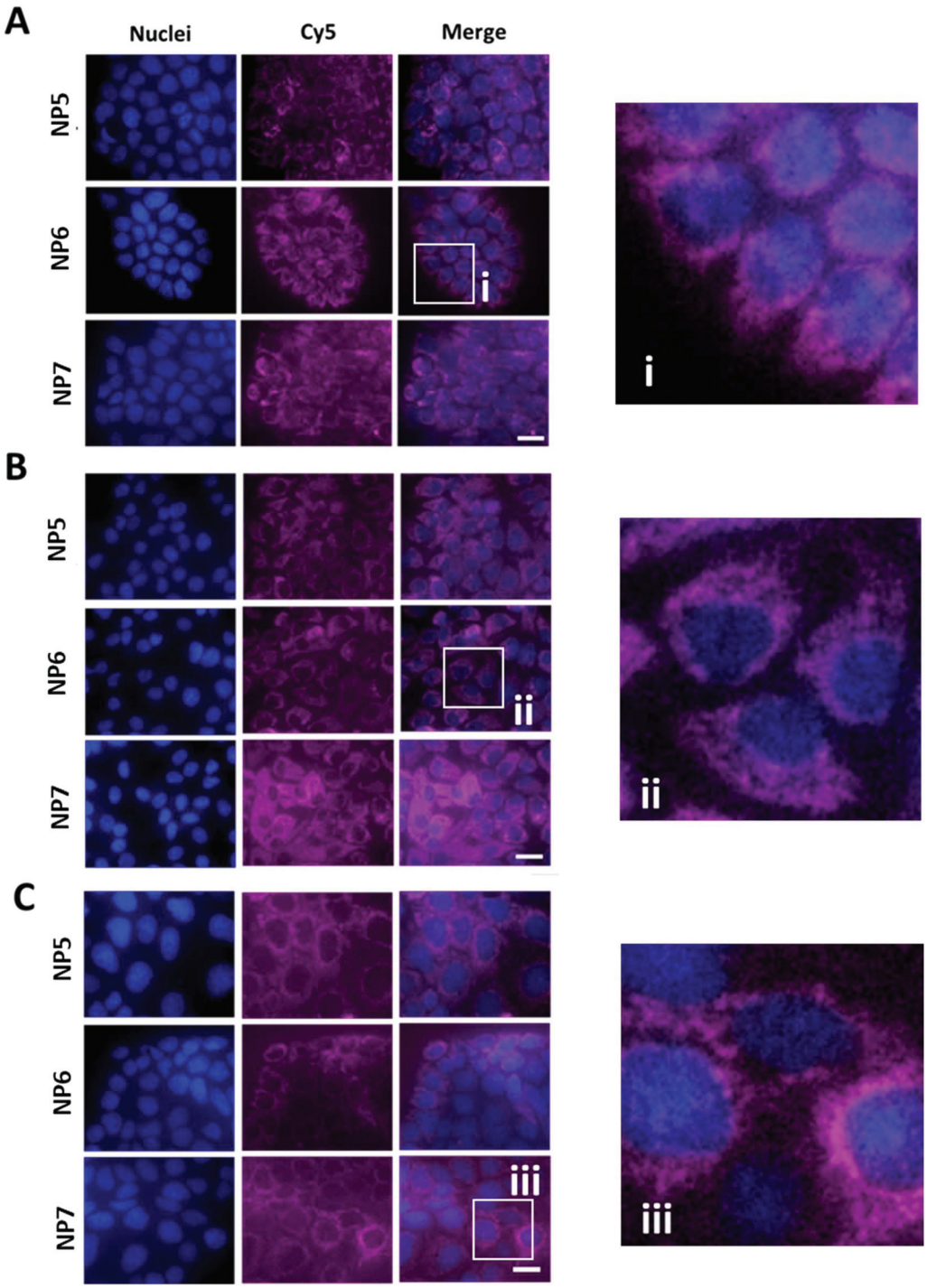

Fig. 4 Micrographs of nanoparticle internalization in (A) A431, (B) A549 and (C) Caco-2 epithelial cells. Cells were incubated with nanoparticle solutions (NPs 5–7) at the concentration of 6.5 × 10 μg mL^{-1} for 120 minutes. (i, ii, iii) Enlarged areas highlighted by light boxes. Scale bar = 30 μm. Images are representative from three independent repeats.

any bimolecular quenching by DOXO on the excited state of NOPD, according to the different localization of these two components in the NPs. This is further supported by the almost unaffected spectral changes observed upon irradiation in the DOXO spectral region (see Fig. 3B) and by the almost unchanged DOXO fluorescence after the irradiation (inset Fig. 3B).

In vitro drug release study

Before testing the pharmacological activity of NPs, the release profile of DOXO contained in the nanoformulations was evaluated at pH 7.4 (blood pH) and 5.0 (approximate lysosomal pH) simulating the body temperature (37 °C). At physiological pH,

 This journal is © The Royal Society of Chemistry 2020

Published on 26 December 2019. Downloaded by Universita Degli Studi di Napoli Federico II on 1/11/2024 3:00:47 PM.

NP1 and NP3 were very stable, in fact, no DOXO release was observed at pH 7.4 in 48 hours. Instead, at pH 5, in the first 24 hours, 4.5% of the anticancer drug was released from NP3, namely 0.34 μg from the initial total cargo of 7.3 μg; after 48 hours the hydrolysis percentage of DOXO from the same NPs was doubled (10.6% released) as shown in Fig. S4.† The trend was slightly different for the mixed micelle NP1, in fact, while after 24 hours the release percentage was around 0.6%, after 48 hours, DOXO release from NP1 was 5.0%, namely 0.6 μg from the initial amount of 11.6 μg (Fig. S4†). These results confirmed the high hydrolytic stability of the urea bond and, at the same time, the acid responsiveness of the designed nanosystem. We designed this nanoformulation specifically so that it would be capable of retaining the drug during circulation in the bloodstream (*i.e.*, pH 7.4), as our prior work had shown that stability of drug-polymer linkers was critical to efficacy in mouse cancer models following systemic injection.[46] We also used the urea linkage as it is sensitive to acidified intracellular compartments (endo/lysosomes, pH *ca.* 5), and because ureas have been evaluated as pro-drugs susceptible to overexpressed proteolytic enzymes in anticancer applications previously.[47] We therefore evaluated the acidic pH triggering of DOXO release as a proxy for the release expected in cell lines and in tumours *in vivo*.[48]

Cell internalization of the NPs

In order to confirm that the designed nanoformulations were able to internalize into cancer cells, fluorescent NPs were prepared by combining the two grafted polymers (P1-DOXO and P1-NOPD in a percentage of 80%) with a fixed amount (20%) of the same polymeric backbone conjugated to Cyanine-5 (P1-Cy5, see Scheme S1†). Three different intrinsically fluorescent NPs were prepared by nanoprecipitation as schematically illustrated in Fig. S5:† NP5, formed by P1-Cy5 and P1-DOXO in a 20/80 ratio, NP6 consisted of P1-Cy5 and P1-NOPD in a 20/80 ratio and the mixed micelle NP7 formed by P1-Cy5, P1-DOXO and P1-NOPD in a 20/40/40 ratio. Incubation of the NPs with lung (A549 adenocarcinoma human alveolar basal epithelial), intestine (Caco-2 human colorectal adenocarcinoma cells) and skin (A431 human epidermoid carcinoma cells) cancer cell lines, representative cell lines for typical PDT candidate tumours, showed internalization of the NPs within 120 minutes as evidenced by the presence of Cy5 fluorescence (Fig. 4A–C).

In all three figures, it can be noted that the Cy5 signal was located in the cytoplasm with an absence of signal in the nuclei of each tested cell line. Further images of the internalized NPs formulations (NP5–7), are separately reported in the ESI (Fig. S6–S8†). In addition to a typically diffuse cytoplasmic signal, bright spots of Cy5 signal were noted during NPs imaging, so a co-localization study in Caco-2 cells was carried out using a lysosomal stain (Lysotracker green). In these images (Fig. 5) the superimposition of the Cy5 and lysosomal marker signals demonstrated that there was some degree of lysosomal accumulation following internalisation. Taken together, these data suggested receptor-mediated endocytosis and trafficking to lysosomes as a possible route of cellular internalization for the mixed-micelle formulation (NP7). Such intracellular trafficking has been widely reported for synthetic polymer NPs,[49,50] and in some cases has been shown to enhance the efficacy of delivered therapeutic agents.[51] We thus anticipated that the new hybrid mixed-micellar-like NPs would release DOXO effectively, after being internalized and trafficked to lysosomes, in accordance with the *in vitro* stability study.

We also performed flow cytometry experiments. Caco-2 cells exposed to the free drug showed augmented fluorescence intensity with increased incubation time (Fig. S9A†). The incubation time did not affect NP3 fluorescence intensity, which was lower than the free drug, but significantly higher than the cell autofluorescence (Fig. S9A†). The free drug presented preferable accumulation in the nuclei of the cells, with 89% cells showing positive colocalization at 4 h, while 20% of cells receiving NP3 showed positive colocalization in the same period (Fig. S9B†). However, the nuclei colocalization of the free drug was significantly affected by the increasing incubation times, which had a ~25% reduction at 48 h (Fig. S9B†). This fact was further evidenced by confocal images, which revealed accumulation of DOXO in cytoplasmic vesicle-like organelles following 48 h incubation with the free drug

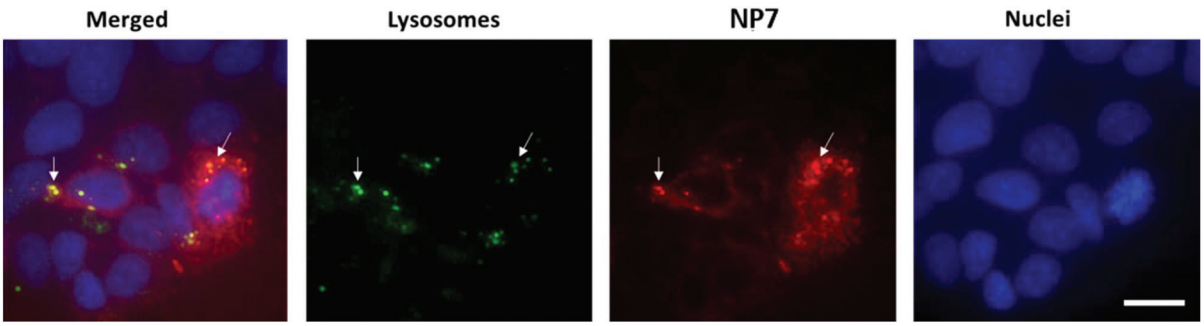

Fig. 5 Co-localization studies in Caco-2 intestinal cells. Cells were treated with a solution 6.5 × 10 μg mL^{-1} of NP7 for 120 minutes. Images were processed on Image J software. Cy5 signal of NP7 was false coloured to red to aid in visualization of co-localization with green lysosomal signal. White arrows indicate regions of green and red overlap. Scale bar = 30 μm.

Published on 26 December 2019. Downloaded by Universita Degli Studi di Napoli Federico II on 1/11/2024 3:00:47 PM.

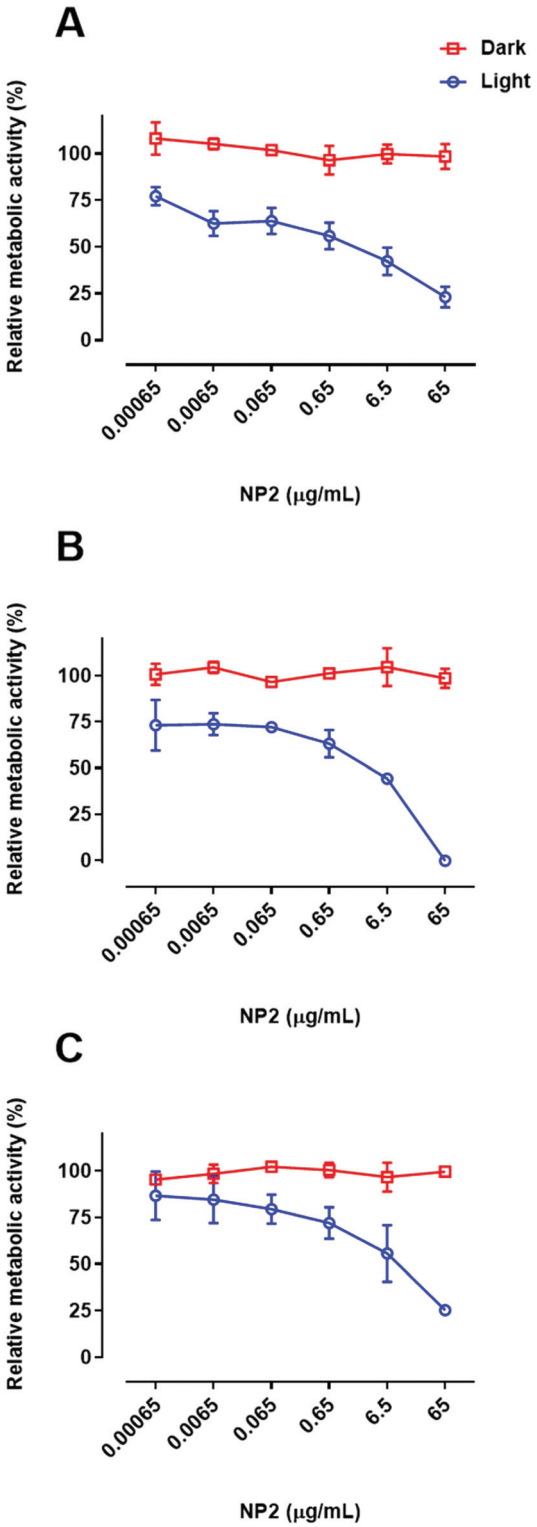

Fig. 6 NP2 light (λ = 400 nm, 7 mW cm^{-2}, for 10 min) *versus* dark effect on cellular metabolic activity by the PrestoBlue assay in (A) A431, (B) A549 and (C) Caco-2 cells. NOPD concentration range is 28.4 × 10^{-6}–28.4 μg mL^{-1}. Cells were exposed to treatments for a total of 48 hours. Data in graphs represent the mean ± S.D. from three independent repeats.

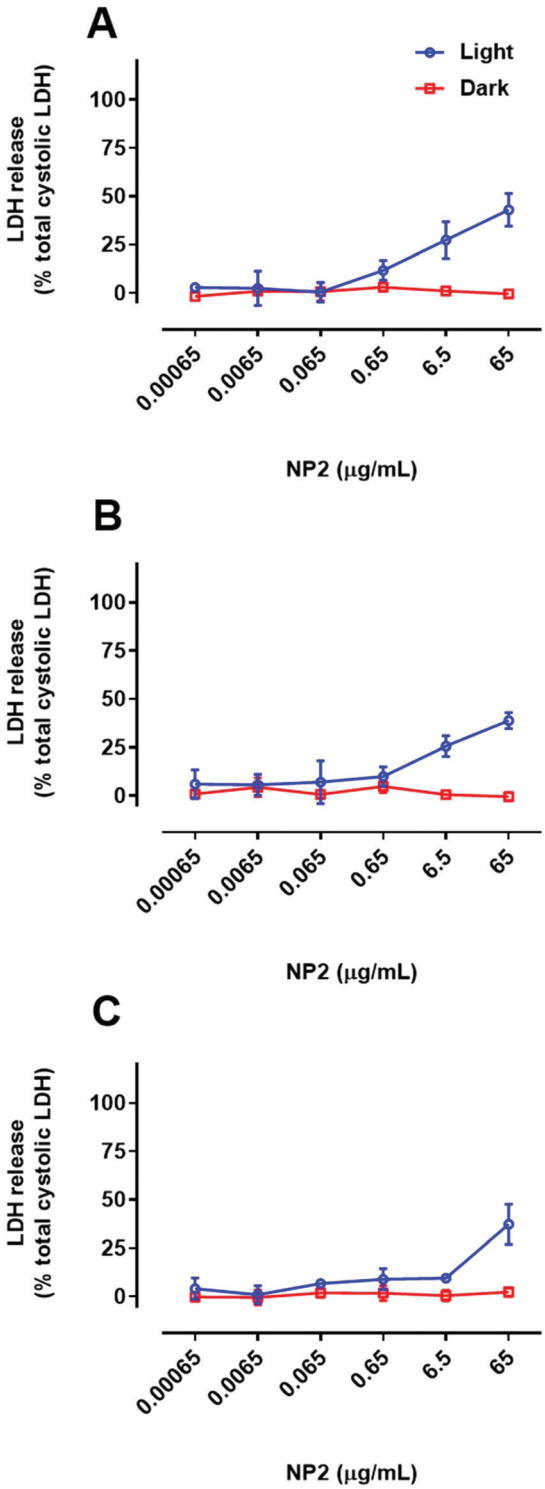

Fig. 7 NP2 light (λ = 400 nm, 7 mW cm^{-2}, for 10 min) *versus* dark effect on the integrity of cell plasma membrane by the LDH assay in (A) A431, (B) A549 and (C) Caco-2 cells. NOPD concentration range is 28.4 × 10^{-6}–28.4 μg mL^{-1}. Cells were exposed to treatments for a total of 48 hours. Data in graphs represent the mean ± S.D. from three independent repeats.

This journal is © The Royal Society of Chemistry 2020

Published on 26 December 2019. Downloaded by Universita Degli Studi di Napoli Federico II on 1/11/2024 3:00:47 PM.

(Fig. S10†). Notably, NP3 presented stable cell uptake and nuclei colocalization at the different time points, whereas the increased incubation time significantly affected the performance of the free drug. It was also important to characterize if DOXO was preferably inside the cell instead of staining the cell membrane and Fig. S9C† shows that both the free drug and NP3 showed good intracellular distribution (ratios of internalization above 1.6) in the different time points.

In vitro toxicity

The cytotoxic profiles of NP1 was studied and compared with NPs 2–4 both in the dark and under light irradiation against all the previously tested cell types (A549, Caco-2 and A431). In the absence of light treatment, NP2 demonstrated no toxicity in the concentration range of 6.5×10^{-4}–6.5×10^{2} μg mL^{-1}, as illustrated in Fig. 6 and 7 (see red line in the figures), and indicated further by the retention of cellular metabolic activity (PrestoBlue assay, Fig. 6A–C) and plasma membrane integrity (lactate dehydrogenase (LDH) release, Fig. 7A–C). In contrast, following light irradiation of 10 minutes' duration, NO was released, with NP2 demonstrating a cell killing effect, observed by both loss of metabolic activity (Fig. 6A–C, blue line) and the release of LDH (Fig. 7A–C, blue line). Assessed *via* metabolic damage (Fig. 6), this effect was observed at the lowest concentration tested (6.5×10^{-4} μg mL^{-1}). A plateau in this effect was noted between 6.5×10^{-4} and 6.5×10^{-1} μg mL^{-1}, before an increase in metabolic damage was observed from 6.5 μg mL^{-1}. Determination of IC_{50} values from metabolic damage revealed that A431 skin cancer cells were the most sensitive to light stimulated NOPD toxicity, and Caco-2 intestinal cancer cells were the most resistant (Table 3).

Table 3 Calculated IC_{50} values by the PrestoBlue assay are for polymer concentration (μg mL^{-1}) and presented as the mean ± S.E.M

	IC_{50} (μg mL^{-1})		
Formulation	A431	A549	Caco-2
NP2 (dark)	>200	>200	>200
NP2 (light)	2.5 ± 1.8	4.2 ± 1.3	8.6 ± 2.4

Interestingly, the release of intracellular LDH, and thus plasma membrane damage, was present at NPs concentrations of ≥6.5 μg mL^{-1} (Fig. 7A–C). Therefore, it was possible that the increased cell killing effect observed in the highest concentrations (≥6.5 μg mL^{-1}), following the plateau in metabolic damage, was due to both mitochondrial and membrane damage caused by the release of NO.[43,44]

The photorelease of NO by NP2 (first row Fig. 8) and also from the mixed micelle (NP1, second row Fig. 8) in all cell lines tested (A431 in the first column, A549 in the second and Caco-2 cells in the third), following irradiation for 10 minutes,

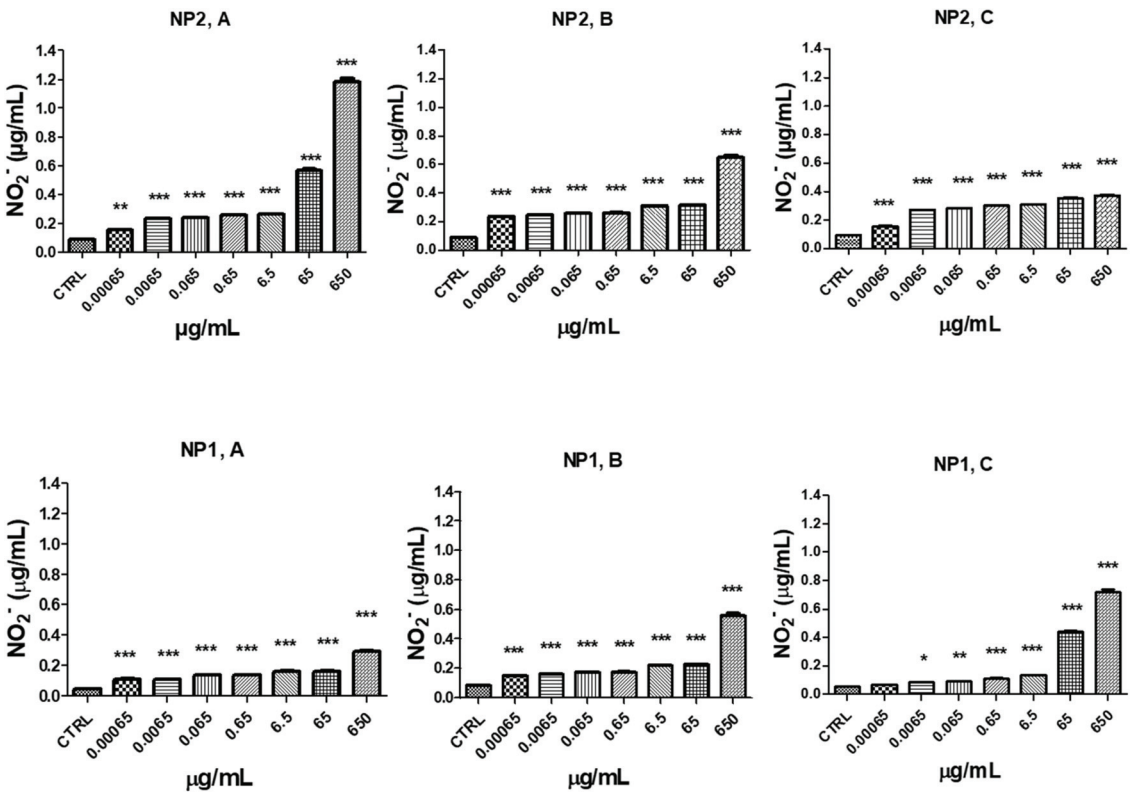

Fig. 8 NO-photorelease in A431 (A), A549 (B) and Caco-2 (C) cells incubated with either NP1 or 2 and either maintained in the dark or irradiated (λ = 400 nm, 7 mW cm^{-2}), for 10 min. Measurements were performed in triplicate and data are presented as means ± S.D. *vs.* untreated cells (ctrl): * $p < 0.05$; ** $p < 0.01$; *** $p < 0.001$.

Published on 26 December 2019. Downloaded by Universita Degli Studi di Napoli Federico II on 1/11/2024 3:00:47 PM.

was studied using the Griess reaction to detect nitrite. The range of concentrations, taken in consideration for each test, of both NPs formulations (NPs 1 and 2) was used also in these experiments and the results are reported in Fig. 8. The NO release was found to be concentration dependent and increased steeply above concentrations of 6.5 μg mL^{-1}.

To investigate the potency and possible enhancement of the chemotherapeutic agent with NOPD, the mixed micelles nanoformulation NP1, formed by P1-NOPD and P1-DOXO, was next tested comparing its performance against free DOXO and NP3 (Fig. 9A–C).

From Fig. 9, it is apparent that also in this case A549 lung cancer cells (Fig. 9B) were the most sensitive to the cell killing effect of free DOXO, and Caco-2 cells (Fig. 9C) were the most resistant. An increase in DOXO potency was achieved *via* the conjugation of DOXO to the P1 and the formulation of polymeric NPs. These increases in DOXO potency were, again, cell type dependent. In particular, in Caco-2 cells (Fig. 9C), the efficacy of nanoformulated DOXO was 8 fold higher than free DOXO. Although with different potency, this trend was also observed in the other two cellular lines (A459 reported in Fig. 9B and A431 cells in Fig. 9A). These data demonstrate that cancer cells more resistant to DOXO treatment, like Caco-2, may benefit the greatest from the nanomedicine approach. The greater efficacy for nanoformulated DOXO compared with the free DOXO is probably due to a different internalization pathway and is in good agreement with the enhanced activity of anticancer drugs observed in polymer micelles.[52,53]

In the absence of light irradiation, it was observed that the NP1 formulation displayed similar IC_{50} values to those of NP3 (Table 4); supporting the previous findings shown in Fig. 6 and 7 that light stimulation was required for the cell toxicity induced by NOPD. It can be noted that under blue light irradiation, the potency of NP1 increased by 5.5-, 2.3- and 1.9-fold for Caco-2 (Fig. 9C), A549 (Fig. 9B) and A431 (Fig. 9A) cells, respectively, compared to the same formulation in the dark (Fig. 9). It can thus be inferred that the increased potency with light stimulation was a result of NOPD and its subsequent release of NO. This was further confirmed by irradiating NP3 and using the same experimental conditions. As shown in Fig. S11,† no cytotoxic effect was seen for the non-light-responsive NP3.

The ultimate comparison of the sequence of formulations tested was between free DOXO solutions and NP1 following stimulation with light, whereby increases in potency of 27.6-, 5.7- and 3.9-fold were achieved in Caco-2 (Fig. 9C), A549 (Fig. 9B) and A431 (Fig. 9A) cells, respectively. Furthermore, to demonstrate potential synergism, combination index (CI) values were calculated using the median-effect algorithm established by Chou and Talalay[54,55] (see experimental) and were based on the potency of NP2 (NOPD-polymer, with light stimulation), NP3 (DOXO-polymer) and the mixed micelle formulation NP1 (NOPD-polymer and DOXO-polymer, with light stimulation). Using this method, CI values of 0.40, 0.56 and 0.83 were calculated for Caco-2, A549 and A431 cells, respectively. Importantly, all CI values represent an indication of synergism (CI < 0.9), and that Caco-2 and A549 cells demonstrate strong synergism (CI < 0.7),[54,55] with the NP1 treatment compared to the effects of the constituent polymer formulations alone. This improvement of cytotoxic effect thus confirmed that the developed hybrid-mixed-micelle-like NP system not only offered the benefit of a temporal control of NO delivery and its therapeutic effect, but it also assured the enhanced activity of DOXO in cell lines curable with NO-phototherapy.

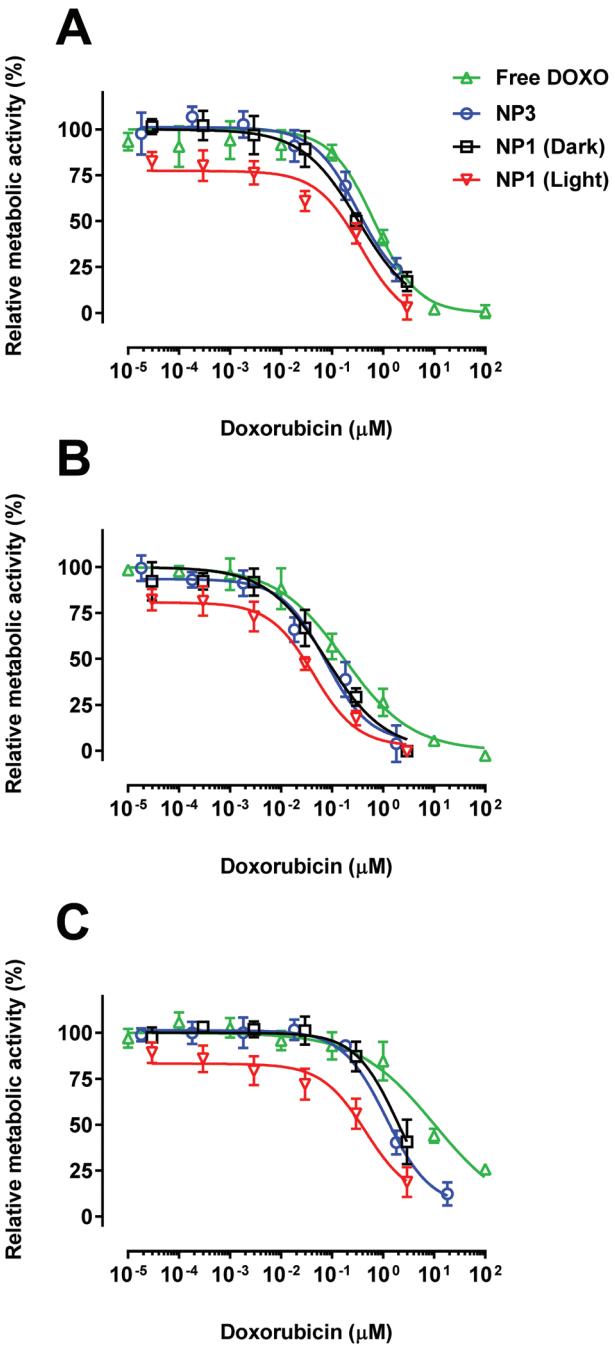

Fig. 9 Dose–response curves of free DOXO, NP3 and NP 1 both in the dark and light conditions in (A) A431, (B) A549 and (C) Caco-2 cells. Data in graphs represent the mean ± S.D. from three independent repeats. Irradiation conditions were the same (λ = 400 nm, 7 mW cm^{-2}, for 10 min).

This journal is © The Royal Society of Chemistry 2020

Published on 26 December 2019. Downloaded by Universita Degli Studi di Napoli Federico II on 1/11/2024 3:00:47 PM.

Table 4 Calculated IC_{50} values are for DOXO concentration and presented as the mean ± S.E.M

	IC_{50} (μM)		
Formulation	A431	A549	Caco-2
Free Doxo	0.7 ± 0.2	0.17 ± 0.02	10.2 ± 2.5
NP3	0.4 ± 0.1	0.07 ± 0.04	1.2 ± 0.2
NP1 (dark)	0.33 ± 0.03	0.07 ± 0.02	2.0 ± 0.6
NP1 (light)	0.2 ± 0.10	0.03 ± 0.01	0.4 ± 0.2

Conclusions

We have demonstrated how the use of hybrid-mixed-micelle-like NPs can be a valid strategy for the enhancement of the antitumor effect of DOXO. In particular, conjugation and formulation of DOXO to polymeric NP3 increases itself the activity of the chemotherapeutic drug if compared with the free form, confirming that polymeric prodrugs may be adopted as enhancers of active molecules in other pharmaceutical and medical applications. This activity is significantly enhanced in the case of the mixed-nanoformulation (NP1) containing both DOXO and the NOPD due to a combination effect in which the increased efficiency of the NO photorelease within the NPs and the slow-release of DOXO play a key role. From the data gathered it can be deduced that when applied together, the photoregulated release of NO alongside the delivery of DOXO, achieves a synergistic effect that confers an enhanced killing ability of cancer cells. To our knowledge, this represents the first example of combination therapy based on chemotherateutics and light-stimulated release of NO achieved by using polymer NP formulations. Therefore, the present work is a promising proof-of-concept suitable for further *in vivo* investigation and, at the same time, may open up the field towards the implementation of this type of hybrid-mixed-micellar systems in biomedical applications.

Experimental section

Chemicals

All chemicals were used as obtained without additional purification unless otherwise stated. *N*,*N*′-Disuccinimidyl carbonate (DSC, ≥95%), poly(ethylene glycol) methyl ether (M_n 5000 Da), 1,8-diazabicyclo[5.4.0]undec-5-ene (DBU, 98%), triethylamine (TEA, ≥99%), di-*tert*-butyl dicarbonate (99%), extra-dry DMSO were purchased from Sigma-Aldrich. 2-Amino-1,3-propanediol (Serinol, 98%) and dichloromethane (DCM, 99.8%, extra dry over molecular sieve, stabilised, Acroseal) were purchased from AcrosOrganics. Trifluoroacetic acid (TFA, 99%) was purchased from VWR Chemicals. Ethylchloroformate was purchased from Merck KGaA. Cyanine5 amine (Cy-5) was purchased from Lumiprobe Life Science Solutions. All reactions involving air-sensitive reagents were performed under nitrogen using oven-dried glassware and the syringe-septum cap technique. Anhydrous sodium sulfate (Na_2SO_4) was used as the drying agent for the organic phase. Organic solvents were removed under reduced pressure at 30 °C. All deuterated solvents used for NMR studies were of spectrophotometric grade.

Synthesis

All syntheses, involving NOPD and DOXO, were carried out under a low intensity level of visible light. NOPD,[39] and P1 were prepared according to previously published protocols.[36] ^{1}H NMR spectra were recorded on a Bruker 400 MHz spectrometer using $CDCl_3$ or DMSO-d_6 as the solvent, as stated. Chemical shifts are expressed in parts per million (δ) downfield from the internal standard tetramethylsilane. The following abbreviations are used to designate peak multiplicity: s = singlet, d = doublet, dd = doublet of doublets; ddd = doublet of doublet of doublets; q = quartet; t = triplet, m = multiplet, bs = broad singlet.

BOC deprotection optimisation

A predetermined amount of protected block co-polymer P1 was dissolved in extra dry DCM. TFA (5 equivalents in excess compared to repeating tBSC units)[56] was added slowly to P1 mixture at 0 °C. The reaction mixture was left stirring for 6 minutes. Following a first precipitation in cold hexane, the resultant material (P1*) was washed with cold diethyl ether and analysed by ^{1}H NMR. NMR samples were taken before the addition of TFA, after 6 minutes (before the precipitation) and post purification and drying. For simplicity, the ^{1}H NMR spectra before the addition of TFA and after the purification and drying process are reported. ^{1}H NMR (t = 0 min) (400 MHz, DMSO-d_6) δ = 5.26–5.10 (m, 80H), 4.17–4.01 (m, 168H), 3.52 (s, 492H), 1.48 (s, 240H), 1.39 (s, 370H). ^{1}H NMR (post purification and drying) (400 MHz, DMSO-d_6) δ = 8.42 (bs, 18H), 7.18–7.02 (m, 34H), 5.24–5.11 (m, 62H), 3.51 (s, 492H), 1.55–1.41 (m, 204H), 1.38 (s, 320H); [14% deprotection].

NOPD coupling procedure (P1-NOPD)

DSC (1.2 eq. with respect to the amount of NOPD, 0.798 mmol, 205 mg) was added to a solution of NOPD (1.0 eq., 0.665 mmol, 175 mg) dissolved in anhydrous MeCN (5 mL) at 0 °C. TEA (1.2 eq. with respect to the amount of NOPD, 0.798 mmol, 111 μL) was added slowly to the reaction mixture and left stirring for 3 hours. Deprotected polymer P1* (1.0 eq., 0.665 mmol, 120 mg; equivalents were calculated to be in varying degrees of excess compared to each repeating tBSC unit) was dissolved in anhydrous MeCN (3 mL) and TEA (2.0 eq. with respect to the amount of P1*, 1.33 mmol, 185 μL) was added, and the solution was subsequently added dropwise to the previous reaction mixture. The reaction was left stirring for a further 3 hours at 0 °C. The resultant conjugated polymer P1-NOPD was purified through multiple precipitation steps in cold hexane : diethyl ether : isopropanol mixture and dialysed against water : methanol mixture for 24 hours. Finally, the purified aqueous suspension was freeze-dried for 48 hours and stored at −22 °C. A final NMR spectrum of the product (P1-NOPD) post purification and completely dried was

Published on 26 December 2019. Downloaded by Universita Degli Studi di Napoli Federico II on 1/11/2024 3:00:47 PM.

recorded. ^{1}H NMR (400 MHz, DMSO-d_6) δ = 8.08 (d, J = 9.2 Hz, 10H), 7.06 (bs, 10H), 7.60–7.55 (m, 16H), 6.89–6.76 (m, 10H), 5.25–4.99 (m, 70H), 4.19–3.89 (m, 118H), 3.78 (qd, J = 9.9, 6.0 Hz, 40H), 3.51 (s, 492H), 1.81–1.72 (m, 20H), 1.50–1.42 (m, 180H), 1.38 (s, 142H).

Doxorubicin coupling procedure (P1-DOXO)

DSC (1.5 eq. with respect to the amount of DOXO, 0.125 mmol, 32 mg) pre-dissolved in anhydrous MeCN (3 mL) was added to a solution of DOXO (1.0 eq., 0.083 mmol, 48 mg) in dry DMSO (3 mL) at 0 °C. TEA (2.5 eq. with respect to the amount of DOXO, 0.21 mmol, 30 μL) was added slowly to the reaction mixture and left stirring for 4–5 hours. Deprotected polymer P1* (1.0 eq., 0.083 mmol, 15 mg; equivalents were calculated to be in high excess when compared to each repeating tBSC unit) was dissolved in a mixture of anhydrous MeCN/dry DMSO (50/50, v/v, 3 mL) and TEA (2.0 eq. with respect to the amount of P1*, 0.166 mmol, 23 μL) was added, and the solution was subsequently added dropwise to the previous reaction mixture. The reaction was left stirring for a further 3 hours at 0 °C. The resultant conjugated polymer P1-DOXO was purified through multiple precipitation steps in cold hexane : diethyl ether : isopropanol mixture and dialysed against water : methanol mixture for 24 hours. Finally, the purified aqueous suspension was freeze-dried for 48 hours and stored at −22 °C. A final NMR spectrum of the product (DOXO-polymer) post purification and completely dried was recorded. ^{1}H NMR (400 MHz, DMSO-d_6) δ = 14.08 (s, 4H), 7.93 (d, J = 4.3 Hz, 8H), 7.69–7.65 (m, 4H), 7.63 (s, 4H), 7.07 (d, J = 7.1 Hz, 21H), 5.34 (d, J = 8.7 Hz, 8H), 5.24–5.11 (m, 78H), 4.86 (d, J = 5.9 Hz, 4H), 4.61–4.56 (m, 4H), 4.50 (d, J = 10.1 Hz, 8H), 4.36 (d, J = 4.0 Hz, 12H), 4.16–3.93 (m, 205H), 3.81–3.74 (m, 8H), 3.71–3.66 (m, 4H), 3.51 (s, 492H), 3.24 (s, 4H), 3.07–3.01 (m, 8H), 2.94 (d, J = 5.9 Hz, 4H), 2.23 (d, J = 3.8 Hz, 4H), 1.50–1.41 (m, 200H), 1.38 (s, 290H).

Cy-5 coupling procedure (P1-Cy5)

Protected polymer P1 (1.0 eq., 0.005 mmol, 50 mg), TEA (0.5 mL of a stock solution prepared by dissolving 30 μL of TEA in 3.0 mL anhydrous MeCN) and DSC (1 mL of a stock solution prepared by dissolving 15 mg of DSC in 6 mL anhydrous MeCN) were stirred in a dry glass vial at 0 °C for 3 hours. Cy5-TEA (1 mL of a stock solution prepared by dissolving 3 mg of Cy5 and 10 μL of TEA in 6 mL of anhydrous MeCN) was added to the reaction mixture at 0 °C and left for a further for 3 hours. The resultant conjugated polymer P1-Cy5 was purified through multiple precipitation steps in cold hexane : diethyl ether mixture and subsequently dialysed against water : methanol mixture for 24 hours. Finally, the purified aqueous suspension was freeze-dried for 48 hours and stored at −22 °C.

Nanoparticle preparation

The nanoprecipitation method was used to form NPs, whereby the grafted copolymers were dissolved in acetone at concentrations of either 1 mg mL^{-1} or 5 mg mL^{-1} (final concentration in water/PBS), according to the biological assay to be performed. The polymeric solution was added at a rate of 2 mL min^{-1} to either deionized water or PBS, under constant stirring (550 rpm). The polymers rapidly formed nanoparticle suspensions through solvent exchange between water and acetone. The final suspension was then left stirring for 2 hours and subsequently dialyzed against PBS or water overnight. The same procedure was adopted for the fabrication of NP1 (P1-DOXO/P1-NOPD, 50/50, w/w); NP2, (P1-NOPD/P1, 50/50, w/w), NP3, (P1-DOXO/P1, 50/50, w/w), NP4, (P1, 100%).

Cy5 micelles for cellular uptake experiments

The nanoprecipitation method was used to form mixed nanoformulations combining a fixed amount of P1-Cy5 (20%) with functionalized polymer (P1-DOXO, P1-NOPD or both, 80%) in order to tune the final fluorescence intensity and maximize both materials usage and detection properties (cell uptake and organs biodistribution). The following polymers P1-Cy5/P1-DOXO, P1-Cy5/P1-NOPD, P1-Cy5/P1-DOXO/P1-NOPD were dissolved in acetone, respecting the abovementioned ratios, at concentrations of 1 mg mL^{-1} or 5 mg mL^{-1} (final concentration in water/PBS), according to the biological assay to be performed. The polymeric solution was added at a rate of 2 mL min^{-1} to either deionized water or PBS, under constant stirring (550 rpm). The polymers rapidly formed coloured-nanoparticle suspensions through solvent exchange between water and acetone. The final suspension was then left stirring for 2 hours and dialyzed against water or PBS overnight. The same procedure was adopted for the fabrication of NP5, (P1-Cy5/P1-DOXO, 20/80, w/w), NP6 (P1-Cy5/P1-NOPD, 20/80, w/w), NP7 (P1-Cy5/P1-DOXO/P1-NOPD, 20/40/40, w/w).

Physicochemical characterization

The particle size was analyzed by dynamic light scattering (DLS) using a Zetasizer Nano ZS (Malvern Instruments Ltd) or a Viscotek 802 DLS with a laser wavelength of 830 nm at 20 °C. Polymer solutions were prepared at 1 mg mL^{-1} in PBS. Data was analyzed using OmniSIZE software. A minimum of 10 measurements were collected per sample. Measurements from Zetasizer Nano ZS were taken in triplicate and used to calculate average intensity particle size distributions. The zeta potential of NPs was evaluated according to the electrophoretic mobility of the particles and calculated by the Helmholtz-Smoluchowsky equation. All measurements were performed in triplicate. Samples were measured on a NanoDrop 2000c (Thermo Scientific) for UV or a NanoDrop 3300 (Thermo Scientific) for fluorescence. DOXO content in the micelles was calibrated against DOXO standards (λ_{exc} = 580 nm, λ_{em} = 553 nm) and NOPD content in the micelles was calibrated against NOPD standards (λ = 405 nm) using UV. Cy5 content in the mixed micelles was calibrated against Cy5-amine standards (λ_{exc} = 647 nm, λ_{em} = 665 nm) using fluorescence.

In vitro doxorubicin release study

Drug release studies were performed in phosphate buffer saline (PBS) at pH 7.4 (blood pH) and citrate phosphate buffer (0.1 M citric acid, 0.2 M Na_2HPO_4) at pH 5 (to mimic the lyso-

 This journal is © The Royal Society of Chemistry 2020

Published on 26 December 2019. Downloaded by Universita Degli Studi di Napoli Federico II on 1/11/2024 3:00:47 PM.

some pH). A sample (500 μL) of NPs 1 and 3 was placed in a dialysis device (Slide-A-Lyzer mini dialysis device, 3.5 K MWCO, Thermo Scientific). The micellar solution was dialyzed against 1.5 mL of release media at 37 °C and samples (0.2 mL) were collected at appropriate time points and replaced with the same amount of fresh medium to maintain sink conditions. The released DOXO from collected samples was quantified by RP-HPLC analysis as previously described.[57]

Griess assay

NO release was evaluated, as nitrite formed, using the Griess reaction. 5 mL of NPs 1 and 2 were irradiated using a violet led 10 W lamp. An irradiance of 7 mW cm^{-2} was measured with an HD2302.0 Delta Ohm light meter equipped with a Delta Ohm LP471RAD light probe. The presence of nitrite was determined at regular time intervals using the Griess assay; where 1.0 mL of the reaction mixture was treated with 250 μL of Griess reagent (4% w/v sulphanilamide, 0.2% w/v *N*-naphthylethylenediamine dihydrochloride, 1.47 M phosphoric acid). After 15 min at room temperature, the reaction mixture was analysed spectrophotometrically and calibration curves obtained with standard solutions of sodium nitrite at 0.5 μM to 50 μM ($r^2 > 0.99$). The nitrite yield was expressed as amount of NO_2^- (μg mL^{-1}, relative to the initial compound concentration) ± SEM.

Instrumentations

UV-Vis spectra absorption were either recorded on a Varian Cary 50BIO UV/Vis spectrophotometer (Varian Australia Pty Ltd, Mulgrade, Australia), or on a JascoV-560 spectrophotometer, while fluorescence emission spectra were recorded on a Spex Fluorolog-2 (mod. F-111) spectrofluorimeter. UV-Vis and fluorescence emission spectra were performed all in air-equilibrated solutions, using quartz cells with a path length of 1 cm. Absorption spectral changes were monitored by irradiating the sample in a quartz cell (1 cm path length, 3 mL capacity), using a continuum laser with λ_{exc} = 405 nm (*ca.* 100 mW) having a beam diameter of *ca.* 1.5 mm. Fluorescence lifetimes were recorded with the same fluorimeter equipped with a TCSPC Triple Illuminator. The samples were irradiated by a pulsed diode excitation source (Nanoled) at 455 nm. The kinetics were monitored at 525 nm and each solution itself was used to register the prompt at 455 nm. The system allowed measurement of fluorescence lifetimes to be carried out from 200 ps. Irradiation of the samples in solution was performed in a thermostated quartz cells (1 cm pathlength, 3 mL capacity) under gentle stirring, by using a continuum laser with λ_{exc} = 405 nm (*ca.* 100 mW) having a beam diameter of *ca.* 1.5 mm.

Direct monitoring of NO release for samples in solution was measured by amperometric detection with a World Precision Instrument, ISO-NO meter, equipped with a data acquisition system, and based on direct amperometric detection of NO with short response time (<5 s) and sensitivity range 1 nM–20 μM. The analogue signal was digitalized with a four-channel recording system and transferred to a PC. The sensor was accurately calibrated by mixing standard solutions of $NaNO_2$ with 0.1 M H_2SO_4 and 0.1 M KI according to the following reaction:

$$4H^+ + 2I^- + 2NO_2^- \rightarrow 2H_2O + 2NO + I_2$$

Irradiation was performed in a thermostated quartz cell (1 cm path length, 3 mL capacity) using the continuum laser mentioned above at λ_{exc} = 405 nm. NO measurements were carried out under stirring with the electrode positioned outside the light path in order to avoid NO signal artefacts due to photoelectric interference on the ISO-NO electrode.

Biological experiments

Chemicals

Culture media were supplied by Sigma Chemical Co (St Louis, MO) and plasticware for cell cultures was from Corning (New York, USA). The protein content of cell lysates was assessed with the BCA kit from Sigma Chemical Co (St Louis, MO). Unless otherwise specified, all the reagents were from Sigma Chemical Co.

Cells

A431 human epidermoid carcinoma cells, A549 adenocarcinomic human alveolar basal epithelial cells and Caco-2 human colorectal adenocarcinoma cells were purchased from the American Type Tissue Collection (ATCC) and used at passages 20–30, 30–40 and 35–45, respectively. All cells were cultured in Dulbecco's Modified Eagle's Medium (DMEM; Sigma-Aldrich) supplemented with 10% (v/v) Fetal Bovine Serum (FBS; Sigma-Aldrich), 0.1 mg mL^{-1} streptomycin, 100 units per mL penicillin, 0.25 μg mL^{-1} amphotericin (Sigma-Aldrich) and 2 mM L-glutamine (Sigma-Aldrich) at 37 °C with 5% CO_2. Cells were seeded at a density of 1×10^4 cells per well in 96 well plates (Corning) for 24 hours prior to assaying. Dosing of cells was initiated by removing culture medium, washing cells with phosphate buffered saline (PBS; Sigma-Aldrich) and the application of 100 μL per well of treatment for 48 hours. Treatment solutions were applied to cells diluted in DMEM (no phenol red; Thermo-Fisher) supplemented as described above, however with the lack of antibiotics in the medium. Cells were treated with solutions of plain polymeric NPs (NP4), NOPD-conjugated polymeric NPs (NP2, at concentrations of 6.5×10^{-4} to 6.5×10^2 μg mL^{-1}), DOXO-conjugated polymeric NPs (NP3), mixed micelle formulations of NOPD- and DOXO-conjugated polymeric NPs (NP1), or free DOXO (DOXO concentrations of 1×10^{-5} to 1×10^2 μM). In all *in vitro* experiments, treatment with DMEM alone served as the negative control and 1.0% (v/v) Triton X-100 diluted in DMEM as the positive cell death control. When indicated, cells were exposed to the light emitted by a 400 nm, 10 W LED for 10 minutes, using an irradiance of 7 mW cm^{-2}, at room temperature. Non-irradiated cells were maintained in a dark room for 10 minutes at room temperature. After light irradiation, cells were incubated for 48 hours at 37 °C with 5% CO_2 before the assaying described below were applied.

Published on 26 December 2019. Downloaded by Universita Degli Studi di Napoli Federico II on 1/11/2024 3:00:47 PM.

Cytotoxicity testing

Plasma membrane integrity was studied by detecting for released lactate dehydrogenase (LDH) in the extracellular environment. Following the incubation with treatments, 75 μL per well of supernatant was removed from the treated cells and transferred to a 96 well plate. 150 μL per well of LDH detection reagent (TOX7 kit; Sigma-Aldrich) was then added to the samples and the resulting solution was incubated at room temperature for 25 minutes in the dark. Absorbance was measured at 492 nm. Relative LDH release was calculated by setting the absorbance value of the negative control as 0% and the positive control (1.0% Triton X-100) as 100%. PrestoBlue Cell Viability Reagent (Thermo-Fisher) was used to assess the metabolic activity of cells following treatments. Following exposure, treatment solutions were removed, cells were washed with PBS and 100 μL per well of 10% PrestoBlue reagent diluted in DMEM (no phenol red) was applied to cells for 60 minutes. Solution fluorescence was then measured at 560/600 nm ($\lambda_{exc}/\lambda_{em}$), and relative metabolic activity calculated by setting the values of the negative control as 100% and the positive control (1.0% Triton X-100) as 0%.

Determination of combination index (CI) values

CI values were determined according to a widely used method established by Chou and Talalay.[54,55] Calculated IC_{50} values were used in the following equation to determine CI values:

$$CI = \frac{D_{CA}}{D_{SA}} + \frac{D_{CB}}{D_{SB}} + \frac{D_{CA}D_{CB}}{D_{SA}D_{SB}}$$

where D_{CA} represents the IC_{50} values (based on NOPD concentration) of NP1 (mixed micelles of NOPD-polymer and DOXO-polymer), and D_{SA} the IC_{50} (based on NOPD concentration) of NP2 (micelles of NOPD-polymer). Similarly, D_{CB} represents the IC_{50} values of (based on DOXO concentration) of NP1 (mixed micelles of NOPD-polymer and DOXO-polymer), and D_{SB} the IC_{50} (based on DOXO concentration) of NP3 (micelles of DOXO-polymer). Based on this method, CI values are indicative of strong synergism (<0.7), synergism (0.7–0.9), additive effect (0.9–1.1), antagonism (1.1–3.3), or strong antagonism (>3.3).[54,55]

Nitrite release in the cells

The amount of extracellular nitrite was measured spectrophotometrically. Nitrite production was measured by adding 12.5 μL of Griess reagent (1 : 1 solution of 0.2% w/v naphthylethylenediamine dihydrochloride, and 2% w/v sulphanilamide in 5% v/v phosphoric acid) to 50 μL samples of cell supernatant per well in a 96-well plate. After a 15 min incubation at 37 °C in the dark, absorbance was measured at 540 nm with a Packard EL340 microplate reader (Bio-Tek Instruments, Winooski, VT). Sodium nitrite was used as a standard to generate the calibration curve ($r^2 > 0.99$). Nitrite concentration was expressed as amount of NO_2^- (μg mL^{-1}, relative to the initial nanoparticle concentration) ± S.E.M.

Cellular internalization experiments

To investigate cellular uptake, live cell fluorescent microscopy of NPs 5–7 was performed on Caco-2, A431 and A549 cells. Cells were incubated with nanoparticle solutions for 120 minutes followed by three washes with ice cold PBS to remove particles. Cells were then stained with either 6 μg mL^{-1} Hoechst 33342 (Thermo-Fisher) or 6 μg mL^{-1} Hoechst 33342 and 100 nM Lysotracker green (Thermo-Fisher) applied in PBS for 30 minutes. Staining solution was removed and cells washed twice with PBS. FluoroBrite DMEM media (Thermo-Fisher) was added to wells and cells were imaged on an inverted Nikon Eclipse TE 300 fluorescent microscope on DAPI and Cy5 filters. Images were merged using Image J software.

Confocal. Caco-2 cells were exposed to NP3 and free drug at 1 μM DOXO for 4/24/48 h. Then, cells were washed with warm PBS and incubated with Hoechst 33342 nuclei stain (5 μg mL^{-1}) for 10 minutes. In sequence, the cells were washed with warm PBS and incubated with PBS containing 4% PFA for 15 min at room temperature. The preserved cells were washed with warm PBS and kept in PBS. Images were acquired in a TCS SPE Leica confocal microscope using 20× objective and the images were analysed using ImageJ software.

Imaging flow cytometry. Caco-2 cells were exposed to NP3 and free drug at 1 μM doxorubicin for 4/24/48 h. Control samples included cells receiving no treatment and single stain controls (NP3/doxorubicin/Hoechst 33342). After 4/24/48 h incubation time, the treatments were removed and the cells washed with warm PBS. Then, cells receiving Hoechst 33342 nuclei stain were incubated with the dye solution in cell culture media (2 μg mL^{-1}) for 10 minutes. Cells were washed with warm PBS, detached using trypsin-EDTA solution and resuspended in PBS containing 4% PFA. After incubation with the PFA solution for 15 min at room temperature, the cells were centrifuged and resuspended in 50 μL PBS. Samples were analysed in an Image Streamx Mk II Imaging Flow Cytometer (Amnis®) with 40× magnification. The data analysis was performed in an IDEAS® Image Stream Analysis Software (Amnis®).

Statistical analysis

Dose–response curve fitting was performed using non-linear regression analysis to enable IC_{50} determination (GraphPad prism, version 7.03). Statistical analysis was performed by one-way ANOVA with Dunnett's multiple comparison *post hoc* test using GraphPad Prism.

Conflicts of interest

The authors declare no competing financial interest.

Acknowledgements

This work is supported by grants from Italian Association for Cancer Research (AIRC) IG-19859, by the Engineering and Physical Sciences Research Council [grant numbers EP/N006615/1, EP/L01646X/1, EP/N03371X/1]; and the Royal Society [Wolfson Research Merit Award WM150086] (to CA).

 This journal is © The Royal Society of Chemistry 2020

Published on 26 December 2019. Downloaded by Universita Degli Studi di Napoli Federico II on 1/11/2024 3:00:47 PM.

References

1 (*a*) J. A. Kemp, M. S. Shim, C. Y. Heo and Y. J. Kwon, *Adv. Drug Delivery Rev.*, 2016, **98**, 3–18; (*b*) S. Shen, M. Liu, T. Li, S. Lina and R. Mo, *Biomater. Sci.*, 2017, **5**, 1367–1381.

2 (*a*) Y. Li, K. Atkinson and T. Zhang, *Cancer Lett.*, 2017, **396**, 103–109; (*b*) M. Hou, P. Xue, Y.-E. Gao, X. Ma, S. Bai, Y. Kang and Z. Xu, *Biomater. Sci.*, 2017, **5**, 1889–1897.

3 M. A. Dawson, *Science*, 2017, **355**, 1147–1152.

4 J. Lehar, A. S. Krueger, W. Avery, A. M. Heilbut, L. M. Johansen, E. R. Price, R. J. Rickles, G. F. Short, J. E. Staunton, X. Jin, M. S. Lee, V. Zimmermann and A. A. Borisy, *Nat. Biotechnol.*, 2009, **27**, 659–666.

5 S. Bai, X. Ma, X. Shi, T. Zhang, Y. Wang, Y. Cheng, P. Xue, Y. Kang and Z. Xu, *ACS Appl. Mater. Interfaces*, 2019, **11**, 36130–36140.

6 W. Q. Liu, S. Z. F. Phua and Y. L. Zhao, *ACS Appl. Mater. Interfaces*, 2019, **11**, 31638–31648.

7 Y. Lim, Y. W. Xu, Z. Z. Zhang, Y. Y. Hiuo, D. X. Chen, W. Ma, K. Sun, G. Y. Tonga, G. D. Zhou, D. S. Kohane and K. Tao, *Nano Lett.*, 2019, **19**, 5515–5523.

8 For a recent review see: F. Quaglia and S. Sortino, in *Applied Photochemistry. Lecture Notes in Chemistry*, ed. S. G. Bergamini and S. Silvi, Springer, Switzerland, 2016, vol. 92, pp. 397–426.

9 S. Sortino, *J. Mater. Chem.*, 2012, **22**, 301–318.

10 A. P. Castano, P. Mroz and M. R. Hamblin, *Nat. Rev. Cancer*, 2006, **6**, 535–545.

11 (*a*) J. P. Celli, B. Q. Spring, I. Rizvi, C. L. Evans, K. S. Samkoe, S. Verma, B. W. Pogue and T. Hasan, *Chem. Rev.*, 2010, **12**, 2795–2838; (*b*) J. Zhang, D. Si, S. Wang, X. Chen, H. Zhou and M. Yang, *Biomater. Sci.*, 2019, **7**, 2468–2479; (*c*) W. Park, S. Cho, J. Han, H. Shin, K. Na, B. Lee and D.-H. Kim, *Biomater. Sci.*, 2018, **6**, 79–90.

12 S. Sortino, *Chem. Soc. Rev.*, 2010, **39**, 2903–2913.

13 P. C. Ford, *Nitric Oxide*, 2013, **34**, 56–65.

14 N. L. Fry and P. K. Mascharak, *Acc. Chem. Res.*, 2011, **44**, 289–298.

15 C. Parisi, M. Failla, A. Fraix, B. Rolando, E. Gianquinto, F. Spyrakis, E. Gazzano, C. Riganti, L. Lazzarato, R. Fruttero, A. Gasco and S. Sortino, *Chem. – Eur. J.*, 2019, **25**, 1080–11084.

16 M. Blangetti, A. Fraix, L. Lazzarato, E. Marini, B. Rolando, F. Sodano, R. Fruttero, A. Gasco and S. Sortino, *Chem. – Eur. J.*, 2017, **23**, 9026–9029.

17 A. D. Ostrowski and P. C. Ford, *Dalton Trans.*, 2009, **48**, 10660–10669.

18 *Nitric Oxide: Biology and Pathobiology*, ed. L. J. Ignarro, Elsevier Inc., 2009, ISBN: 9780123738660.

19 D. Fukumura, S. Kashiwagi and R. K. Jain, *Nat. Rev. Cancer*, 2006, **6**, 521–534.

20 A. Bishop and J. E. Anderson, *Toxicology*, 2005, **208**, 193.

21 D. A. Wink and J. B. Mitchell, *Free Radicals Biol. Med.*, 1998, **25**, 434–456.

22 S. Moncada and J. D. Erusalimsky, *Nat. Rev. Mol. Cell Biol.*, 2002, **3**, 214–220.

23 D. A. Wink, Y. Vodovotz, J. Laval and M. Laval, *Carcinogenesis*, 1998, **19**, 711–721.

24 C. Riganti, E. Miraglia, D. Viarisio, C. Costamagna, G. Pescarmona, D. Ghigo and A. Bosia, *Cancer Res.*, 2005, **65**, 516–525.

25 S. De Boo, J. Kopecka, D. Brusa, E. Gazzano, L. Matera, D. Ghigo, A. Bosia and C. Riganti, *Mol. Cancer*, 2009, **8**, e108.

26 P. G. Wang, M. Xian, X. Tang, X. Wu, Z. Wen, T. B. Cai and A. J. Janczuk, *Chem. Rev.*, 2002, **102**, 1091.

27 P. G. Wang, T. B. Cai and N. Taniguchi, *Nitric oxide donors*, Widely-VCH Verlag GmbH & Co. KGaA, Weinhheim, Germany, 2005.

28 C. Fowley, A. P. McHale, B. McCaughan, A. Fraix, S. Sortino and J. F. Callan, *Chem. Commun.*, 2015, **51**, 81–84.

29 A. Fraix and S. Sortino, *Photochem. Photobiol. Sci.*, 2018, **17**, 1709–1727.

30 K. Chegaev, A. Fraix, E. Gazzano, G. E. F. Abd-Ellatef, M. Blangetti, B. Rolando, S. Conoci, C. Riganti, R. Fruttero, A. Gasco and S. Sortino, *ACS Med. Chem. Lett.*, 2017, **8**, 361–365.

31 G. Minotti, P. Menna, E. Salvatorelli, G. Cairo and L. Gianni, *Pharmacol. Rev.*, 2004, **56**, 185–229.

32 J. Swaminathan, A. Garcia-Amros, A. Fraix, N. Kandoth, S. Sortino and F. M. Raymo, *Chem. Soc. Rev.*, 2014, **43**, 4167–4178.

33 A. Fraix, V. Kirejev, M. Malanga, E. Fenivesi, S. Beni, M. B. Ericson and S. Sortino, *Chem. – Eur. J.*, 2019, **23**, 7091–7095.

34 P. Couvreur, *Adv. Drug Delivery Rev.*, 2013, **65**, 21–23.

35 V. Taresco, C. Alexander, N. Singh and A. K. Pearce, *Adv. Ther.*, 2018, **1**, 1800030.

36 C. E. Vasey, A. K. Pearce, F. Sodano, R. Cavanagh, T. Abelha, V. Cuzzucoli Crucitti, A. B. Anane-Adjei, M. Ashford, P. Gellert, V. Taresco and C. Alexander, *Biomater. Sci.*, 2019, **7**, 3832–3845.

37 A. K. Pearce, C. E. Vasey, A. B. Anane-Adjei, F. Sodano, D. J. Irvine, S. M. Howdle, C. Alexander and V. Taresco, *Macromol. Chem. Phys.*, 2019, 1900270.

38 E. B. Caruso, S. Petralia, S. Conoci, S. Giuffrida and S. Sortino, *J. Am. Chem. Soc.*, 2007, **129**, 480–481.

39 F. L. Callari and S. Sortino, *Chem. Commun.*, 2008, **17**, 1971–1973.

40 A. Fraix, N. Marino and S. Sortino, *Top. Curr. Chem.*, 2016, **370**, 225–257.

41 H. Phan, R. I. Minut, P. McCrorie, C. Vasey, R. R. Larder, E. Krumins, M. Marlow, R. Rahman, A. Alexander, V. Taresco and A. K. Pearce, *J. Polym. Sci., Part A: Polym. Chem.*, 2019, **57**, 1801–1810.

42 H. Xiao, H. Song, Q. Yang, H. Cai, R. Qi, L. Yan, S. Liu, Y. Zheng, Y. Huang, T. Liu and X. Jing, *Biomaterials*, 2012, **33**, 6507–6519.

43 P. Taladriz-Blanco and M. G. de Oliveira, *J. Photochem. Photobiol., A*, 2014, **293**, 65–71.

Published on 26 December 2019. Downloaded by Universita Degli Studi di Napoli Federico II on 1/11/2024 3:00:47 PM.

44 I. Di Bari, R. Picciotto, G. Granata, A. R. Blanco, G. M. L. Consoli and S. Sortino, *Org. Biomol. Chem.*, 2016, **14**, 8047–8052.
45 M. Malanga, M. Seggio, V. Kirejev, A. Fraix, I. Di Bari, E. Fenyvesi, M. B. Ericson and S. Sortino, *Biomater. Sci.*, 2019, **7**, 2272–2276.
46 R. M. Englans, J. I. Hare, J. Barnes, J. Wilson, A. Smith, N. Strittmatter, P. D. Kemmitt, M. J. Waring, S. T. Barry, C. Alexander and M. B. Ashford, *J. Controlled Release*, 2017, **247**, 73–85.
47 A. M. Jordan, T. H. Khan, H. Malkin and H. M. I. Osborn, *Bioorg. Med. Chem.*, 2002, **10**, 2625–2633.
48 S. Oelmann, A. Travanut, D. Barther, M. Romero, S. M. Howdle, C. Alexander and M. A. R. Meier, *Biomacromolecules*, 2019, **20**, 90–101.
49 L. Sasso, L. Purdie, A. M. Grabowska, A. T. Jones and C. Alexander, *J. Interdiscip. Nanomed.*, 2018, **3**, 67–81.
50 H. Herd, D. Daum, A. T. Jones, H. Huwer, H. Ghandehari and C. M. Lehr, *ACS Nano*, 2013, **7**, 1961–1973.
51 M. Gulfam, T. Matini, P. F. Monteiro, R. Riva, H. Collins, K. Spriggs, S. M. Howdle, C. Jerome and C. Alexander, *Biomater. Sci.*, 2017, **5**, 532–550.
52 A. V. Kabanov, E. V. Batrakova and V. Y. Alakhov, *J. Controlled Release*, 2002, **82**, 189–212.
53 M. Gulfam, T. Matini, P. F. Monteiro, R. Riva, H. Collins, K. Spriggs, S. M. Howdle, C. Jérôme and C. Alexander, *Biomater. Sci.*, 2017, **5**, 532–550.
54 T. C. Chou, *Pharmacol. Rev.*, 2006, **58**, 621–681.
55 T. C. Chou, *Cancer Res.*, 2010, **70**, 440–446.
56 L. Hedrick, C. A. Pleasanton, V. Shrinivas and V. T. Yi, US0072607A1, 2014.
57 L. Bergandi, E. Mungo, R. Morone, O. Bosco, B. Rolando and S. Doublier, *Front. Pharmacol.*, 2018, **9**, 866.

This journal is © The Royal Society of Chemistry 2020